ELSEVIER

Carbohydrate Research 279 (1995) 59–73

CARBOHYDRATE RESEARCH

Conformational analysis of oligosaccharides corresponding to the cell-wall polysaccharide of the *Streptococcus* group A by Metropolis Monte Carlo simulations

Rainer Stuike-Prill [a], B. Mario Pinto [b,*]

[a] *Department of Chemistry, Carlsberg Laboratory, Gamle Carlsberg Vej 10, DK-2500 Valby, Copenhagen, Denmark*

[b] *Department of Chemistry, Simon Fraser University, Burnaby, B.C. V5A 1S6, Canada*

Received 7 February 1995; accepted in revised form 15 July 1995

Abstract

Metropolis Monte Carlo simulations have been performed on four substructures from the cell-wall polysaccharide antigen of *Streptococcus* group A to explore the conformational behaviour of these compounds. The compounds examined are the trisaccharide, propyl 3-*O*-(2-acetamido-2-deoxy-β-D-glucopyranosyl)-2-*O*-(α-L-rhamnopyranosyl)-α-L-rhamnopyranoside, **1**, the tetrasaccharide, propyl 3-*O*-(3-*O*-(2-acetamido-2-deoxy-β-D-glucopyranosyl)-2-*O*-(α-L-rhamnopyranosyl)-α-L-rhamnopyranosyl)-α-L-rhamnopyranoside, **2**, the hexasaccharide, propyl 3-*O*-(2-*O*-(3-*O*-(3-*O*-(2-acetamido-2-deoxy-β-D-glucopyranosyl)-α-L-rhamnopyranosyl)-α-L-rhamnopyranosyl)-3-*O*-(2-acetamido-2-deoxy-β-D-glucopyranosyl)-α-L-rhamnopyranosyl)-α-L-rhamnopyranoside, **3**, and the hexasaccharide, propyl 3-*O*-(2-acetamido-2-deoxy-β-D-glucopyranosyl)-2-*O*-(3-*O*-(3-*O*-(2-acetamido-2-deoxy-β-D-glucopyranosyl)-2-*O*-(α-L-rhamnopyranosyl)-α-L-rhamnopyranosyl)-α-L-rhamnopyranosyl)-α-L-rhamnopyranoside, **4**. In general, the conformational flexibility of similar glycosidic linkages in different compounds is comparable. However, in a few cases, small differences in the conformations available to these linkages in different structural environments could be detected. Interestingly, a second conformation found for the β-D-GlcNAc-(1 → 3)-α-L-Rha linkage in three of the compounds was not populated in the hexasaccharide **4**. Furthermore, a conformational locale of the α-L-Rha-(1 → 3)-α-L-Rha linkage found to be populated in the trisaccharide **1**, tetrasaccharide **2**, and hexasaccharide **4** is negligibly populated in the hexasaccharide **3**. Ensemble averaged proton–proton distances compare favourably with experimental average distances obtained from NMR spectroscopy. The trisaccharide branch point

* Corresponding author.

SSDI 0008-6215(95)00279-0

in the hexasaccharides is shown to be a highly defined conformational feature. The same unit has been found to be one of the crucial elements recognized by anti-Group A *Streptococcus* antibodies, a result that has implications for the design of improved immunodiagnostics and vaccines.

Keywords: Metropolis Monte Carlo simulations; Cell-wall polysaccharide; Streptococcus group A; Oligosaccharides

1. Introduction

The β-hemolytic *Streptococcus* group A is one of the primary infective agents in humans, causing streptococcal pharyngitis [1]. In certain individuals, untreated or improperly treated infections lead to acute rheumatic fever which in turn, can cause fatal damage to the heart or can lead to long-term lethal effects by scarring heart valves [2]. Evidence to date has suggested that an abnormal immune response to the *Streptococcus* group A infection results in an autoimmune reaction against host tissues. However, the exact mechanism by which the streptococcal infection is linked to the onset and propagation of rheumatic heart disease remains to be resolved [1,2].

As part of a program designed to probe the relationship between streptococcal infections and rheumatic heart disease, we have focused in recent years on the synthesis of oligosaccharide antigens corresponding to the cell-wall polysaccharide of the β-hemolytic *Streptococcus* group A, [3,4] and their use in the selection and characterization of polyclonal and monoclonal antibodies with binding profiles for different epitopes [5]. Glycoconjugates containing the oligosaccharide haptens can serve as a readily accessible source of defined antigens for immunodiagnosis whereas the antibodies can be used in immunohistological studies to probe the origin of the cross-reaction.

Our preliminary immunochemical work [5] indicated that the branch point and the size of the *Streptococcus* antigen appeared to be crucial elements of the epitope recognized by both polyclonal and monoclonal antibodies that also bind the native polysaccharide antigen. An appreciation of the conformations of the oligosaccharides and hence the topographical features presented to antibodies is, therefore, of interest. This information can be derived from NOE/ROE data and heteronuclear $^{3}J_{C-H}$ coupling constants across glycosidic linkages in NMR experiments [6–8]. The complexity of the conformational problem requires, however, a computational approach to complement the experimental results to facilitate the analysis.

In order to examine the role of the branch point and the extended surface of the *Streptococcus* epitope in interactions with antibodies, we present herein the conformational analysis by Metropolis Monte Carlo (MMC) simulations [9,10] of increasingly complex oligosaccharides corresponding to the polysaccharide antigen. A complementary treatment with molecular dynamics simulations, in conjunction with NMR data, has also recently been completed [11]. These approaches serve as first steps in the analysis since it is recognized that conformational changes of the ligand may occur upon binding [12,13]. The computational demands presented by a rigorous molecular mechanics treatment of a multi-parameter system such as that encountered in a hexasaccharide have prompted us to examine the GEGOP force field [14,15] in which only glycosidic

torsional angles, exocyclic torsional angles, and glycosidic valence angles are allowed to vary. The MMC protocol, incorporating the HSEA potential energy functions used in the GEGOP force field, compares favourably to treatments with more sophisticated force fields such as MM2CARB and AMBER [10]. In particular, best agreement with experimental data has been obtained with the former method [10]. A correlation between the ensemble-averaged interproton distances determined from the Monte Carlo simulations and the time-averaged values derived experimentally [11] by ROESY experiments [16,17] is established.

2. Experimental

Computational methods.—All force-field calculations were performed with the GEGOP program [14] Version 2.6, which utilizes a modified HSEA force field [15]. Simulations were carried out in vacuo. The geometry of an oligosaccharide is defined by the following torsional angles: the glycosidic torsional angles ϕ(H-1–C-1–O-1–C-x) and ψ(C-1–O-1–C-x–H-x), where x is the attachment site of the aglycon; exocyclic torsional angles ω(O-6–C-6–C-5–O-5); hydroxyl torsion angles χ; and glycosidic bond angle τ. Bond lengths and bond angles, except for the glycosidic bond angles were kept constant. The β-D-GlcNAc residues adopted a $^4C_1$ chair conformation and the α-L-Rha residues a $^1C_4$ chair conformation. The atomic coordinates of the monosaccharide residues were taken from X-ray structure analysis. The coordinates of the hydrogen atoms were generated according to geometrical criteria.

Metropolis Monte Carlo (MMC) simulations [9,10] were performed over one million steps starting from an energy-minimized conformation. A new conformation was generated by varying all dihedral angles simultaneously. If the energy difference, $\Delta E = E_{new} - E_{old}$, between the newly generated conformation and the previous one was negative, the new conformation was accepted. For $E_{new} > E_{old}$, the Metropolis criterion was applied. Thus, a random number [$Z = 0, 1$] was generated and compared to the Boltzmann factor $\exp(-\Delta E/RT)$, where R = gas constant and T = temperature. If Z was smaller than the Boltzmann factor, the new conformation was accepted, otherwise the old one was counted and used again as the starting point for the next MMC step. Dihedral angles were randomly changed within the following intervals: for tri- and tetra-saccharide, $\Delta\phi$, $\Delta\psi = 20.0°$, $\Delta\omega = 24.0°$, $\Delta\chi = 28.0°$, and for the hexasaccharides, $\Delta\phi$, $\Delta\psi = 14.0°$, $\Delta\omega = 20.0°$, $\Delta\chi = 20.0°$. The glycosidic bond angles were randomly changed in intervals of $\Delta\tau = 3°$. The intervals in which the dihedral angles and the glycosidic bond angles were allowed to change during one MMC step were chosen so that the acceptance ratio was between 30–60%. In the simulations presented in this paper, the acceptance ratio was ca. 41–51%. The conformational energies and the values of all dihedral angles of each calculated conformation were stored and used for further analysis. Tables 1–4 list the dihedral angles with highest population, low and high values, and angle range obtained from the MMC simulations of **1–4**, respectively. The ensemble average distances were averaged as $\langle r^{-6} \rangle^{-1/6}$ values.

The MMC calculations were performed at a simulation temperature of 700 K [18] in order to efficiently sample the conformational space available to the molecule in a finite

Table 1
Dihedral angles with highest population, low and high values, angle range, and % population of the second conformation obtained from MMC simulations of the trisaccharide **1**

Linkage		High pop.	Low	High	Range	Pop. 2nd
B–Propyl						
	ϕ	51	−89	102	191	
	ψ	170	31	−19	310	
A′–B						
	ϕ	42(−30) [a]	−77	96	173	4%
	ψ	18(−23)	−93	85	178	
C–B						
	ϕ	52(168)	−47	−173	126	5%
	ψ	−16(9)	−70	96	167	

[a] Values in parentheses are for the second conformation.

simulation time. The elevated temperature decreases the energy differences between conformers by a factor 2.3 (700/300) which increases the Boltzmann factors of conformers and accordingly their populations. The experimental data represent time-averaged values resulting from an ensemble of conformations populated on the NMR time-scale. Therefore, a theoretical treatment is required that adequately samples the populated conformations if the calculated ensemble-averaged distances are to be compared to those derived experimentally by NMR spectroscopy. MMC simulations of oligosaccharides at 600 K have been shown to lead to a wider sampling of conformational states and have yielded results that show excellent agreement with experimental NOEs [10]. It is worth noting that recent molecular dynamics studies have also shown that higher simulation temperatures are necessary to explore the conformations available to a molecule [19].

Table 2
Dihedral angles with highest population, low and high values, angle range, and % population of the second conformation obtained from MMC simulations of the tetrasaccharide **2**

Linkage		High pop.	Low	High	Range	Pop. 2nd
A–Propyl						
	ϕ	52	−84	101	186	
	ψ	169	23	−35	303	
B–A						
	ϕ	44(−46) [a]	−76	95	171	9%
	ψ	19(−15)	−89	103	192	
A′–B						
	ϕ	44(−15)	−78	95	173	6%
	ψ	21(−33)	−87	83	170	
C–B						
	ϕ	51(163)	−47	−168	121	2%
	ψ	−14(5)	−68	98	166	

[a] Values in parentheses are for the second conformation.

Table 3
Dihedral angles with highest population, low and high values, angle range, and % population of the second conformation obtained from MMC simulations of the hexasaccharide I **3**

Linkage		High pop.	Low	High	Range	Pop. 2nd
A–Propyl						
	ϕ	51	−90	98	188	
	ψ	173	34	−31	295	
B–A						
	ϕ	43(−39) [a]	−64	94	158	11%
	ψ	21(−22)	−91	97	181	
C–B						
	ϕ	53(165)	−46	−171	124	3%
	ψ	−17(5)	−69	102	171	
A′–B						
	ϕ	42	−60	98	158	
	ψ	20	−83	77	160	
B′–A′						
	ϕ	47(−42)	−67	97	164	7%
	ψ	24(−18)	−84	95	179	
C′–B′						
	ϕ	49(171)	−44	−170	126	3%
	ψ	−4(7)	−78	125	203	

[a] Values in parentheses are for the second conformation.

Table 4
Dihedral angles with highest population, low and high values, angle range, and % population of the second conformation obtained from MMC simulations of the hexasaccharide II **4**

Linkage		High pop.	Low	High	Range	Pop. 2nd
B–Propyl						
	ϕ	56	−86	97	183	
	ψ	239	38	−30	293	
A′–B						
	ϕ	44	−35	94	129	
	ψ	20	−84	78	162	
C–B						
	ϕ	51(40) [a]	−42	−179	137	0%
	ψ	−16(151)	−68	169	237	
B′–A′						
	ϕ	45(−41)	−66	94	160	7%
	ψ	19(−19)	−82	106	188	
A–B′						
	ϕ	43(−36)	−62	94	156	5%
	ψ	20(−23)	−80	83	164	
C′–B′						
	ϕ	51	−43	−178	135	
	ψ	−16	−69	86	155	

[a] Values in parentheses are for the second conformation.

Calculations were performed on a Silicon Graphics Indigo workstation, and molecular graphics was done with the Insight software package (Biosym Inc.) on a Personal Iris. The ϕ/ψ plots and trajectories of dihedral angles were generated using the PV-Wave graphics package (Precision Visuals Inc.).

NMR-derived distances.—Proton–proton distances were obtained from ROESY spectra [11]. The cross peaks were integrated and corrected for Hartmann–Hahn and offset effects according to equations given by Bax [20]. After applying these corrections to the integrals, the proton–proton distances were calculated, using the two-spin approximation and assuming isotropic tumbling, according to the following equation, $r_{ij} = R_0(\sigma_0/\sigma_{ij})$, where r_0 is the ruler distance (i.e., the distance between H-1 and H-2 within the same rhamnose ring or between H-1 and H-3 in the *N*-acetylglucosamine ring) and σ_0/σ_{ij} is the ratio of the corresponding cross-relaxation rates. The uncertainty of the cross-peak intensities was $\pm 15\%$. Distances calculated from different data sets showed variations of $\pm 5\%$.

3. Results and discussion

The compounds chosen for study were the trisaccharide, propyl 3-*O*-(2-acetamido-2-deoxy-β-D-glucopyranosyl)-2-*O*-(α-L-rhamnopyranosyl)-α-L-rhamnopyranoside, **1**, the tetrasaccharide, propyl 3-*O*-(3-*O*-(2-acetamido-2-deoxy-β-D-glucopyranosyl)-2-*O*-(α-L-rhamnopyranosyl)-α-L-rhamnopyranosyl)-α-L-rhamnopyranoside, **2**, the hexasaccharide I, propyl 3-*O*-(2-*O*-(3-*O*-(3-*O*-(2-acetamido-2-deoxy-β-D-glucopyranosyl)-α-L-rhamnopyranosyl)-α-L-rhamnopyranosyl)-3-*O*-(2-acetamido-2-deoxy-β-D-glucopyranosyl)-α-L-rhamnopyranosyl)-α-L-rhamnopyranoside, **3**, and the hexasaccharide II, propyl 3-*O*-(2-acetamido-2-deoxy-β-D-glucopyranosyl)-2-*O*-(3-*O*-(3-*O*-(2-acetamido-2-deoxy-β-D-glucopyranosyl)-2-*O*-(α-L-rhamnopyranosyl)-α-L-rhamnopyranosyl)-α-L-rhamnopyranosyl)-α-L-rhamnopyranoside, **4**. The trisaccharide **1** is incorporated in the "reducing"

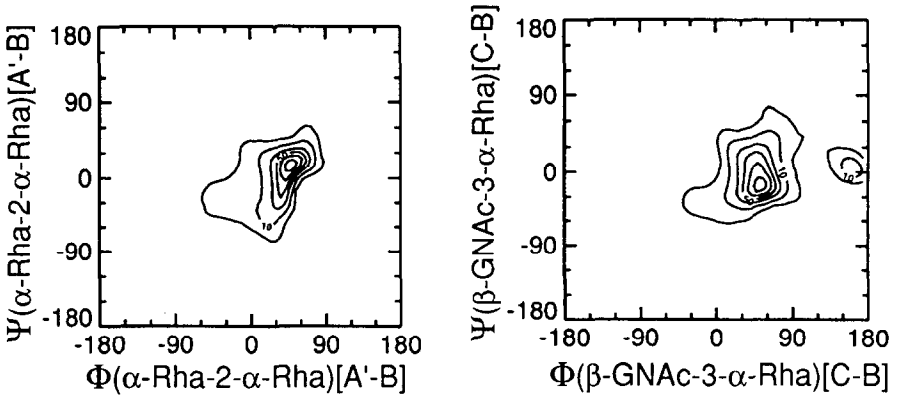

Fig. 1. Population contour maps of the ϕ and ψ dihedral angles of the glycosidic linkages in trisaccharide **1** from an MMC simulation at 700 K. The contour levels are drawn at 1, 10, 30, 50, 70, and 90% relative to the highest population. Levels at 10% and 50% are labelled.

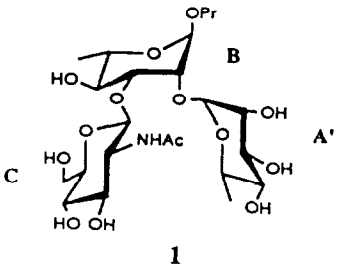

1

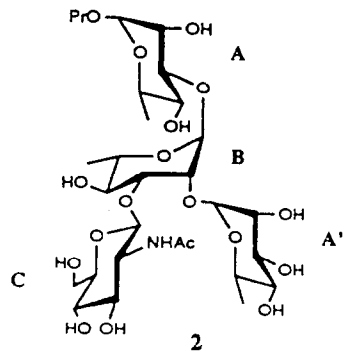

2

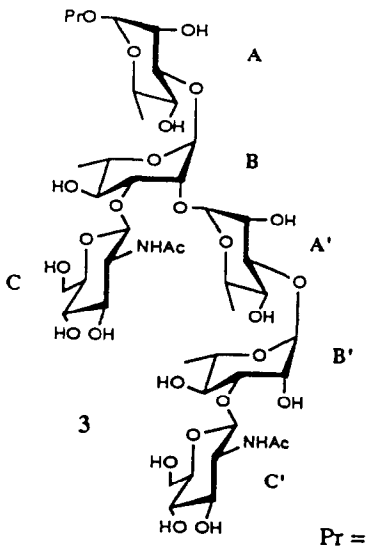

3

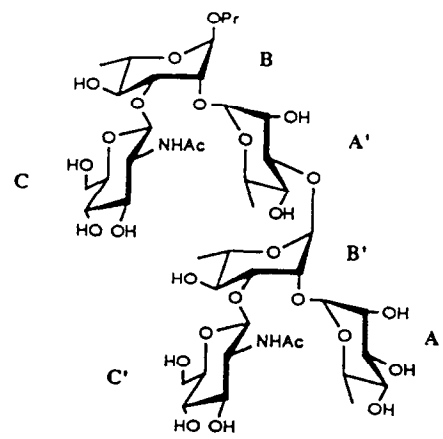

4

Pr = $CH_2CH_2CH_3$

portion of the hexasaccharide II, **4**, and the tetrasaccharide **2** is incorporated in the "reducing" portion of the hexasaccharide I, **3**. The salient features of the computational results for each compound are presented in the following discussion.

Trisaccharide **1**.—The ϕ/ψ population map for the glycosidic linkage α-L-Rha-(1 → 2)-α-L-Rha [A′–B] shows the highest population at 42°/18° (Fig. 1). In the ϕ-dimension, a range of $\pm 40°$ about this conformation is significantly populated. In the ψ-dimension, a wider range is populated, between $-60°$ and 40°, and the extension to negative values is only observed for ϕ-angles smaller than 50°. A broad, lightly populated area is centered around $-30°/-23°$ ($\pm 20°$) and accounts for 6% of the total population.

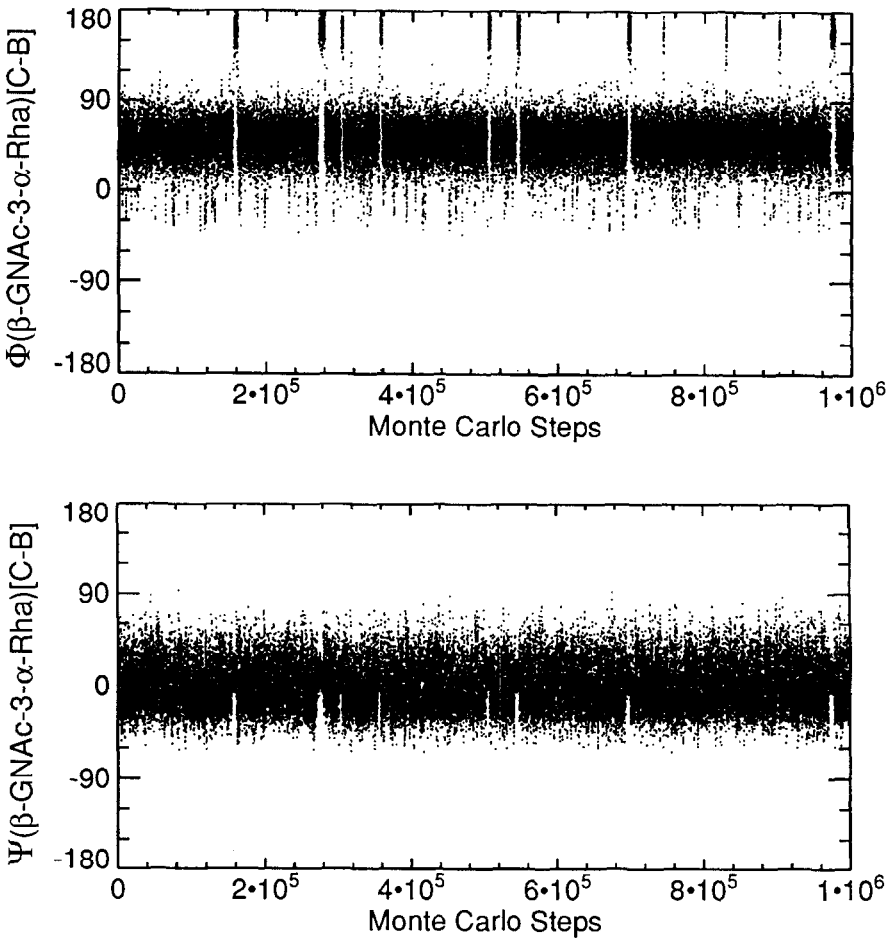

Fig. 2. Variation in ϕ- and ψ-angles for the β-GlcNAc-(1 → 3)-Rha linkage during the MMC simulation of the trisaccharide **1** at 700 K.

The glycosidic linkage β-D-GlcNAc-(1 → 3)-α-L-Rha [C–B] exhibits the highest population at $\phi/\psi = 52°/-16°$ (Fig. 1). A relatively symmetrical area of $\pm 40°$ centred around these values is significantly populated. In the ϕ-dimension, this area extends further to $-60°$. A second distinct conformation can be found around $\phi/\psi = 168°/9°$ with a total population of 5%. The analysis of the values of the ϕ-angle shows that the second conformation was sampled 11 times during the simulation (Fig. 2). At these values of the ϕ-angle, the flexibility about the ψ-angle was significantly reduced (Fig. 2).

Tetrasaccharide **2**.—The ϕ/ψ map of the glycosidic linkage α-L-Rha-(1 → 3)-α-L-Rha [B–A] occupies one major area of population density with the highest population at $\phi/\psi = 44°/19°$ (Fig. 3). The asymmetrical area extends in the ϕ-dimension $\pm 40°$ around the centre. In the ψ-dimension, densely populated areas are found between $-60°$

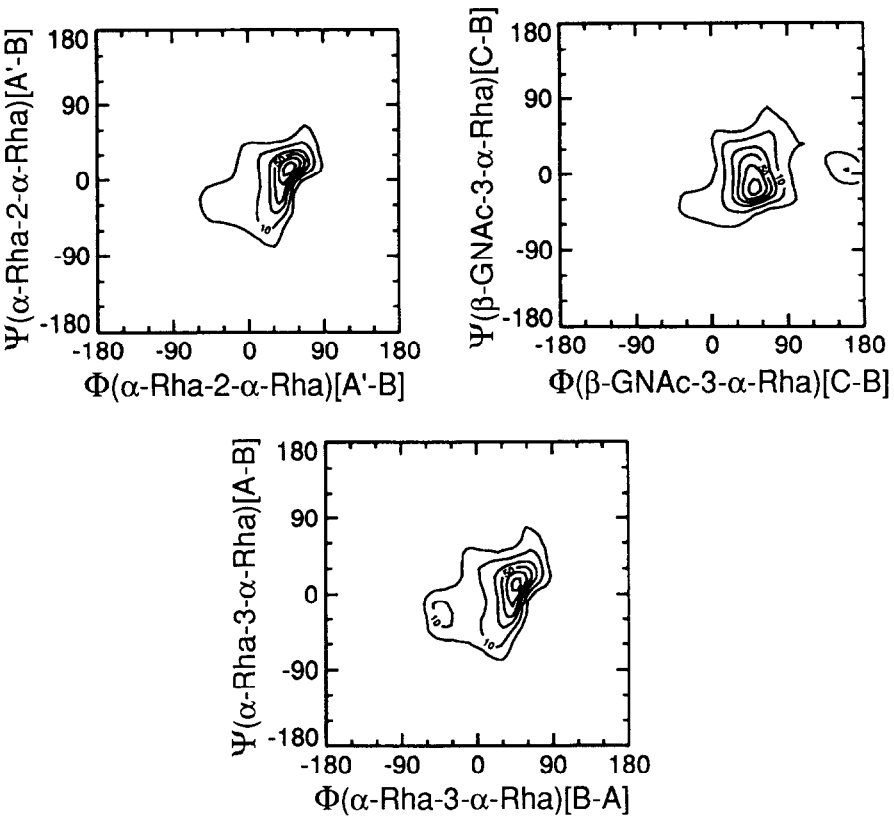

Fig. 3. Population contour maps of the ϕ and ψ dihedral angles of the glycosidic linkages in the tetrasaccharide **2** from an MMC simulation at 700 K. The contour levels are drawn at 1, 10, 30, 50, 70, and 90% relative to the highest population. Levels at 10% and 50% are labelled.

and $+50°$. An additional, lightly populated area is found at $\phi/\psi = -46°/-15°$ which accounts for 9% of the total population.

The ϕ/ψ map of the glycosidic linkage α-L-Rha-(1 → 2)-α-L-Rha [A′–B] shows one major populated area with the highest population at $\phi/\psi = 44°/21°$ (Fig. 3). The distribution about the ϕ- and ψ-angles of this conformation is very similar to that of the linkage [B–A]. However, the lightly populated area centred around $\phi/\psi = -15°/-33°$ is populated to a lower extent (6%). The conformational behaviour of the [A′–B] linkage in **2** is similar to that of the [A′–B] linkage in **1**.

In the ϕ/ψ map of the glycosidic linkage β-D-GlcNAc-(1 → 3)-α-L-Rha [C–B], the area of $\pm 40°$ symmetrically centred around $\phi/\psi = 51°/-14°$ is highly populated (Fig. 3). In the ϕ-dimension, this area extends further to $-60°$. A second conformation can be found around $\phi/\psi = 163°/5°$ with a total population of 2%. The analysis of the values of the ϕ-angle shows that the second conformation was sampled 11 times during the simulation, as for the trisaccharide **1**. At these values, the flexibility about the ψ-angle was significantly reduced. Comparison of the behaviour of the linkage [C–B] in **1** and **2**

reveals that the shapes of the population contour maps are almost identical (Figs. 1 and 2). However, the second conformation is less populated in **2**.

Hexasaccharide I **3**.—The glycosidic linkage α-L-Rha-(1 → 3)-α-L-Rha [B–A] in **3** has its highest population at $\phi/\psi = 43°/21°$ (Fig. 4). An asymmetrical area extends in the ϕ-dimension $\pm 40°$ about the centre. In the ψ-dimension, densely populated areas are found at $+40°$ and $-60°$ from the centre. A second highly populated area is found at $\phi/\psi = -39°/-22°$, accounting for 11% of the total population. A comparison of the ϕ/ψ maps for linkage [B–A] in **3** and in the tetrasaccharide **2**, in which the structural environments are identical, reveals no significant differences either in distribution or in the relative population of the two conformations.

In the ϕ/ψ map of the glycosidic linkage β-D-GlcNAc-(1 → 3)-α-L-Rha [C–B], the area with the highest population is located around $\phi/\psi = 53°/-17°$ (Fig. 4). A relatively symmetrical area of $\pm 40°$ centred around these values is significantly populated. In the ϕ-dimension, this area extends further to $-40°$. A second conformation can be found around $\phi/\psi = 165°/5°$ with a total population of 3%. The analysis of the values of the ϕ-angle shows that the second conformation was sampled three times during the simulation for a few thousand steps. The flexibility of the ψ-angle was significantly reduced at these ϕ values, as also observed for linkage [C–B] in **1** and **2**.

The ϕ/ψ map of the glycosidic linkage α-L-Rha-(1 → 2)-α-L-Rha [A′–B] shows one major populated area with the highest population at $\phi/\psi = 42°/20°$ (Fig. 4). The distribution of the ϕ- and ψ-angles about this point is very similar to the linkage [B–A] in **1** and **2**. However, the area around $\phi/\psi = -25°/-35°$, which was populated in **1** and **2**, is negligibly populated. The ϕ/ψ map of the glycosidic linkage α-L-Rha-(1 → 3)-α-L-Rha [B′–A′] in **3** shows one major area of population density with the highest population at $\phi/\psi = 47°/24°$ (Fig. 4). A second highly populated area is found at $\phi/\psi = -42°/-18°$ which accounts for 7% of the total population. The shape of the contour map is very similar to that of the corresponding linkage [B–A], but the second conformation in [B′–A′] is populated to only half the extent as in linkage [B–A].

The ϕ/ψ map of the glycosidic linkage β-D-GlcNAc-(1 → 3)-α-L-Rha [C′–B′] shows one major populated area with the highest population at $49°/-4°$ (Fig. 4). A relatively symmetrical area of $\pm 40°$ centred around these values is significantly populated. In the ϕ-dimension, this area extends further to $-40°$. A second conformation can be found around $\phi/\psi = 171°/7°$ with a total population of 3%. The analysis of the values of the ϕ-angle shows that the second conformation was sampled three times during the simulation for a few thousand steps. The flexibility of the ψ-angle was significantly reduced at these ϕ values, as already observed for linkage [C–B] in **1** and **2**.

Hexasaccharide II **4**.—The ϕ/ψ map of the glycosidic linkage α-L-Rha-(1 → 2)-α-L-Rha [A′–B] shows one major populated area with the highest population at $44°/20°$ (Fig. 5). The distribution of ϕ- and ψ-angles is very similar to the linkage [A′–B] in **1**, **2**, and **3**. However, the area around $\phi/\psi = -25°/-35°$, which was populated in **1** and **2**, and to a lower extent in **3**, is not populated in **4**. The restriction in conformations for this linkage in **4** can be explained by the different environment of α-L-Rha [A′] in the different oligosaccharides. In **1** and **2**, A′ is located at the non-reducing end whereas in **3**, A′ is linked to B′; in **4**, the B′ residue is linked further to an A residue.

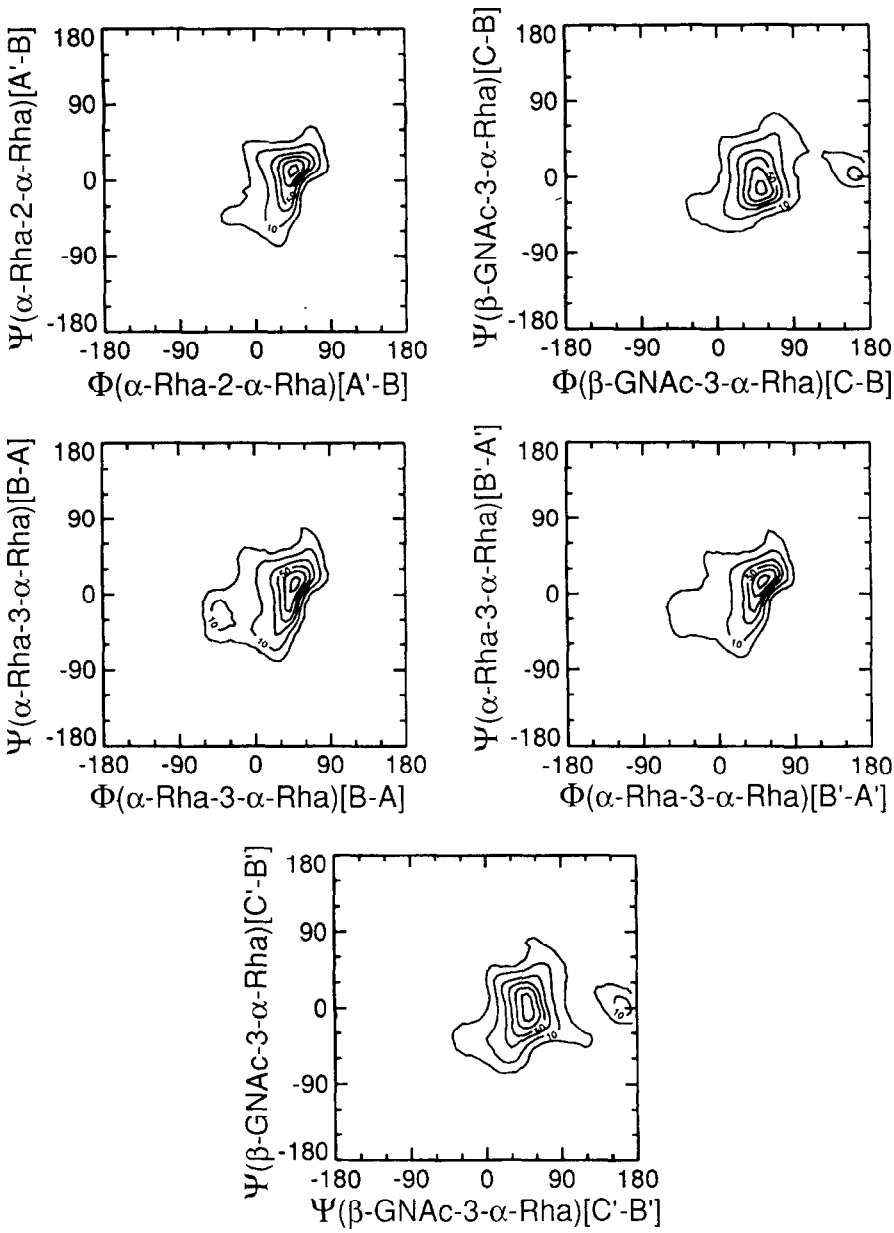

Fig. 4. Population contour maps of the ϕ and ψ dihedral angles of the glycosidic linkages in the hexasaccharide **3** from an MMC simulation at 700 K. The contour levels are drawn at 1, 10, 30, 50, 70, and 90% relative to the highest population. Levels at 10% and 50% are labelled.

The glycosidic linkage β-D-GlcNAc-(1 → 3)-α-L-Rha [C–B] occupies one major area with the highest population at $\phi/\psi = 51°/-16°$ (Fig. 5). The shape of the population contour map is very similar to that of the corresponding linkages in **1**, **2**, and **3**. An

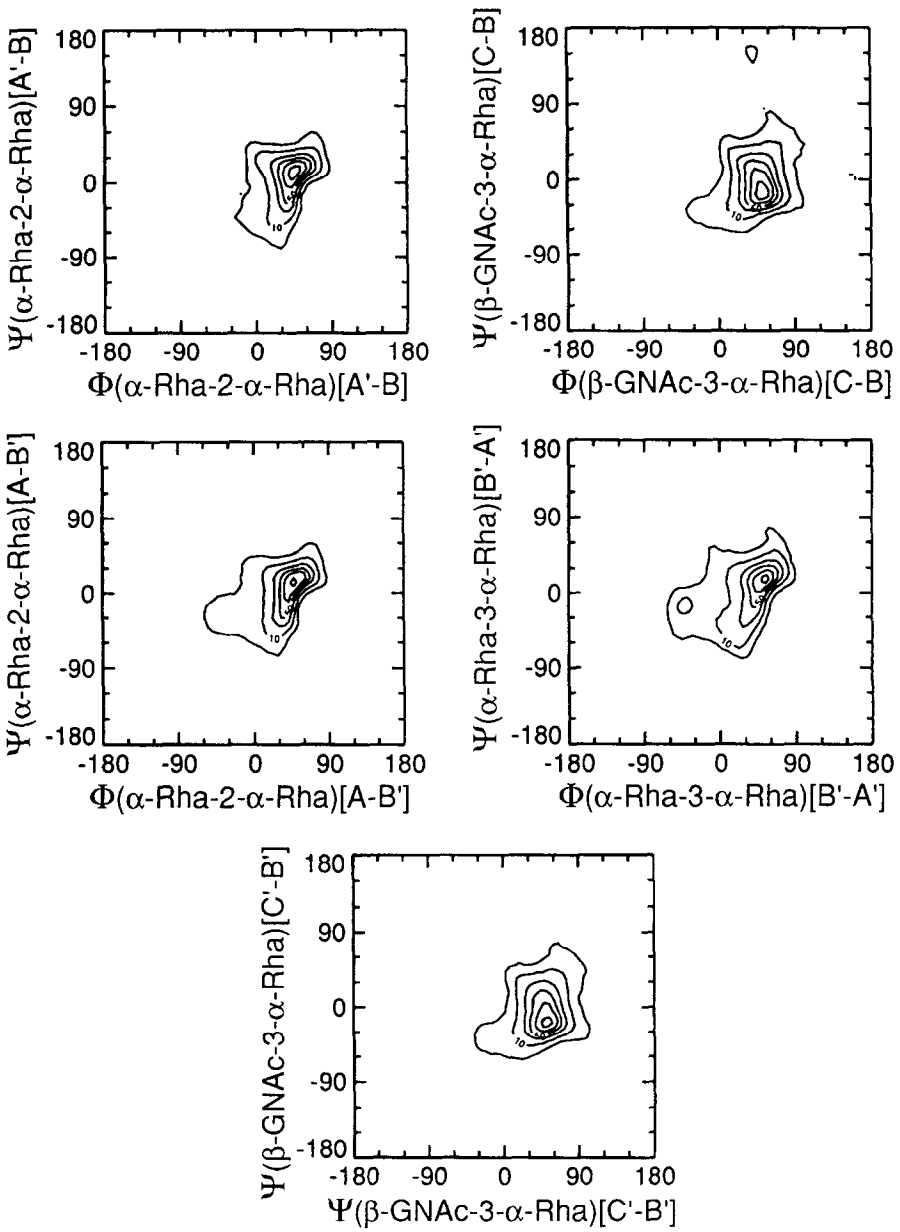

Fig. 5. Population contour maps of the ϕ and ψ dihedral angles of the glycosidic linkages in the hexasaccharide **4** from an MMC simulation at 700 K. The contour levels are drawn at 1, 10, 30, 50, 70, and 90% relative to the highest population. Levels at 10% and 50% are labelled.

additional populated area can be found at $\phi/\psi = 40°/151°$. However, only 0.2% of the total population is found here. It should be noted that in **1**, **2**, and **3** the second conformation resulted from a ϕ-angle around 180° and not from a ψ-angle around 180°, as in **4**.

The ϕ/ψ map of the glycosidic linkage α-L-Rha-(1 → 3)-α-L-Rha [B′–A′] in **4** shows one major area of population density with the highest population at $\phi/\psi = 45°/19°$ and a second highly populated area at $\phi/\psi = -41°/-19°$, which accounts for 7% of the total population (Fig. 5). The overall shape of the population contour map is very similar to that of the corresponding linkage [B–A] in the other oligosaccharides.

The highest population density in the ϕ/ψ map of the glycosidic linkage α-L-Rha-(1 → 2)-α-L-Rha [A–B′] is found around 43°/20° (Fig. 5). The α-L-Rha [A] residue is located at the non-reducing end of the molecule, like the corresponding residue [A′] in linkages [A′–B] in **1** and **2**. Accordingly, the conformations around $\phi/\psi = -36°/-23°$, which were populated in [A′–B] in **1** and **2** but not in **4**, are populated in [A–B′] of **4** (5%).

The conformations sampled for the glycosidic linkage β-D-GlcNAc-(1 → 3)-α-L-Rha [C′–B′] is confined to a broad symmetrical area around $\phi/\psi = 51°/-16°$ (Fig. 5). In contrast to the other β-D-GlcNAc-(1 → 3)-α-L-Rha linkages studied here, no second conformation at ϕ- or ψ-values around 180° was observed for [C′–B′] in **4**.

Rotameric distribution about the C_5–C_6 linkage.—The MMC calculations for all of the oligosaccharides examined indicated that the hydroxymethyl group populated all three staggered conformations with frequent interconversions. The starting point in all cases was −62° (*gg* conformation). The sampling resulted in a rotameric distribution of about 44/40/16% (*gg*/*gt*/*tg*) at 700 K. At 300 K the corresponding ratio was 53/42/5% (*gg*/*gt*/*tg*). The difference in rotameric distribution for the different GlcNAc residues in the oligosaccharides studied was ±3%. The experimental coupling constant data ($^3J_{H\text{-}5,H\text{-}6}$) from NMR spectroscopy [21] are consistent with a high percentage of the *gt* and *gg* conformers [22].

Table 5
Theoretical and experimental ^1H–^1H internuclear distances for tri, tetra-, and hexa-saccharides from the cell-wall polysaccharide of *Streptococcus* Group A

Proton pair	Tri **1**		Tetra **2**		Hexa I **3**		Hexa II **4**	
	MC	Exptl	MC	Exptl	MC	Exptl	MC	Exptl
H-1A–H-1Pr(a)			2.7	2.9	2.7	3.0		
H-1A–H-1Pr(b)			2.5	2.6	2.5	2.7		
H-1A–H-2B′							2.3	2.3
H-1A–H-2C′							3.1	3.1
H-1B–H-3A			2.3	2.2	2.3	2.3		
H-1B–H-5A′	2.3	[a]	2.4	2.4	2.4	2.4	2.4	2.6
H-1B–H-1Pr(a)	2.7	[a]					2.7	2.8
H-1B–H-1Pr(b)	2.5	2.6					2.5	2.4
H-1A′–H-2B	2.3	2.1	2.3	2.4	2.3	2.3	2.3	2.2
H-1A′–H-2C	3.1	2.7	3.1	3.0	3.1	3.5	3.1	3.1
H-1B′–H-5A							2.4	2.6
H-1B′–H-3A′					2.4	2.4	2.3	2.4
H-1C–H-3B	2.4	2.3	2.4	2.3	2.4	2.2	2.4	2.2
H-1C′–H-3B′					2.4	2.2	2.4	2.2

[a] Could not be quantified owing to signal overlap.

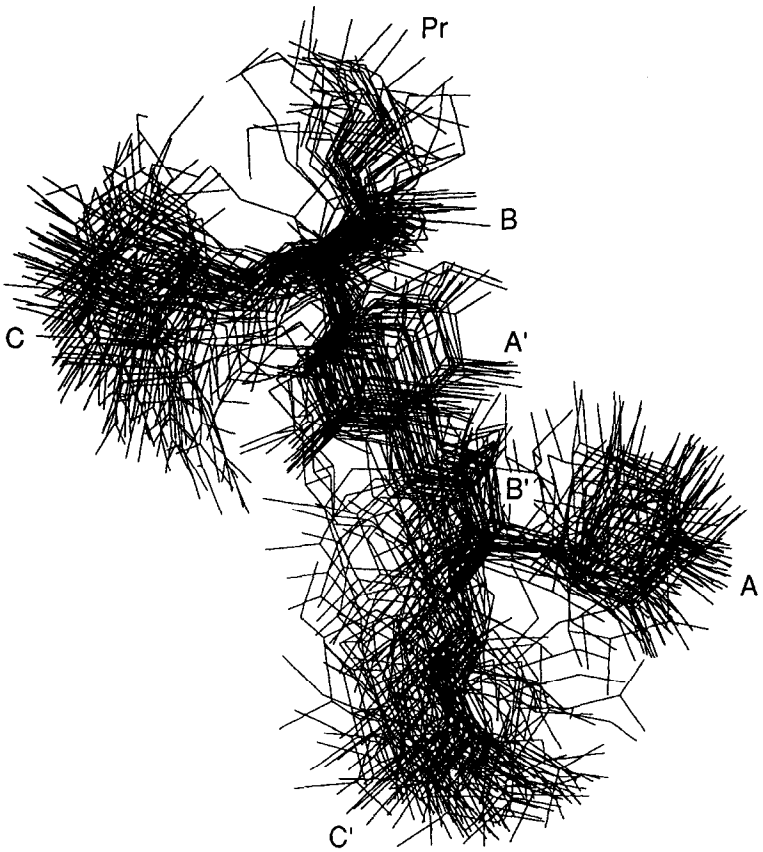

Fig. 6. Overlay of 50 conformers randomly selected from the MMC simulation of the hexasaccharide **4** at 700 K.

A comparison of relevant ensemble-averaged proton–proton distances obtained during the MMC simulation for compounds **1–4** with the corresponding time-averaged distances obtained from NMR spectroscopy [11] is presented in Table 5. Although some discrepancies exist, the agreement is reasonable and lends credence to the validity of the computational method. It should be noted that similar MMC simulations at 600 K have yielded results that are in excellent agreement with experimental NOE data [10].

As a final point of interest, we comment on the flexibility of these oligosaccharides. While the observed scatter in the ϕ/ψ angles is expected, it is noteworthy that, overall, the structures are conformationally restricted. That this is the case is illustrated in Fig. 6 which depicts the superimposition of 50 randomly chosen structures of the hexasaccharide II, **4**. The MMC calculations described here do, however, indicate much higher flexibility about the glycosidic linkages than observed previously with the molecular dynamics calculations [11]. Both models account adequately for the experimental ROE data. Of particular note is the definition of the CBA′ (C′B′A) branched unit. This branch

point has been shown to be a crucial part of the *Streptococcus* group A epitope, together with the extended surface presented by two of these units in the hexasaccharide II, **4** [5,23].

Acknowledgements

We are grateful to the Natural Sciences and Engineering Research Council of Canada for financial support in the form of a grant for research abroad. We also gratefully acknowledge the hospitality of K. Bock of the Carlsberg Laboratory.

References

[1] S.E. Read and J.B. Zabriske (Eds.), *Streptococcal Diseases and the Immune Response*, Academic Press, New York, 1980.
[2] A.L. Bisno, in G.L. Mandell, R.G. Douglas, and J.E. Bennett (Eds.), *Nonsuppurative Poststreptococcal Sequelae: Rheumatic Fever and Glomerulonephritis; Principles and Practice of Infectious Diseases*, 2nd ed., Wiley, New York, 1985, pp 1133–1142.
[3] B.M. Pinto, in P.J. Garegg and A.A. Lindberg (Eds.), *ACS Symp. Ser. 519 on Carbohydrate Antigens*, American Chemical Society, Washington, DC, 1992, pp 111–131, and references cited therein.
[4] J.-R. Marino-Albernas, S.L. Harris, V. Varma, and B.M. Pinto, *Carbohydr. Res.*, 245 (1993) 245–257.
[5] K.B. Reimer, M.A.J. Gidney, D.R. Bundle, and B.M. Pinto, *Carbohydr. Res.*, 232 (1992) 131–142.
[6] S.W. Homans, *Progr. NMR Spectroscopy*, 22 (1990) 55–81.
[7] C.A. Bush and P. Cagas, *Adv. Biophys. Chem.*, 2 (1992) 149–180.
[8] B. Meyer, in J. Thiem (Ed.), *Topics in Current Chemistry*, Vol. 1, Springer, Berlin, 1990, pp 141–208.
[9] N. Metropolis, A.W. Rosenbluth, M.N. Rosenbluth, A.H. Teller, and E. Teller, *J. Chem. Phys.*, 21 (1953) 1087–1092.
[10] T. Peters, B. Meyer, R. Stuike-Prill, R. Somorjai, and J.-R. Brisson, *Carbohydr. Res.*, 238 (1993) 49–73.
[11] U.C. Kreis, V. Varma, and B.M. Pinto, *Int. J. Biol. Macromol.*, 17 (1995) 117–130.
[12] C.P.J. Glaudemans, L. Lerner, G.D. Davies, Jr, P. Kováč, R. Venable, and A. Bax, *Biochemistry*, 29 (1990) 10906–10911.
[13] D.R. Bundle, H. Baumann, J.-R. Brisson, S.M. Gagne, A. Zdanov, and M. Cygler, *Biochemistry*, 33 (1994) 5183–5192.
[14] R. Stuike-Prill and B. Meyer, *Eur. J. Biochem.*, 194 (1990) 903–919.
[15] H. Thogersen, R.U. Lemieux, K. Bock, and B. Meyer, *Can. J. Chem.*, 60 (1982) 44–57.
[16] A.A. Bothner-By, R.L. Stephens, J.-M. Lee, C.D. Warren, and R.W. Jeanloz, *J. Am. Chem. Soc.*, 106 (1984) 811–813.
[17] A. Bax and D.B. Davis, *J. Magn. Reson.*, 63 (1985) 207–213.
[18] L. Poppe, R. Stuike-Prill, B. Meyer, and H. van Halbeek, *J. Biomol. NMR*, 2 (1992) 109–136.
[19] B.M. Pettitt, T. Matsunaga, F. Al-Obeidi, C. Gehrig, V.J. Hruby, and M. Karplus, *Biophys. J.*, 60 (1991) 1540–1544; B.C. Wilkes and P.W. Schiller, *Int. J. Peptide Protein Res.*, 40 (1992) 249–254; Y. Sun and P.A. Kollman, *J. Comput. Chem.*, 13 (1992) 33–40.
[20] A. Bax, *J. Magn. Reson.*, 77 (1988) 134–147.
[21] V. Varma, Ph.D. Thesis, Simon Fraser University, Burnaby, B.C., Canada, 1993.
[22] Y. Nishida, H. Ohrui, and H. Meguro, *Tetrahedron Lett.*, (1974) 1575–1578; C.A.G. Haasnoot, F.A.A.M. de Leeuw, and C. Altona, *Tetrahedron*, 36 (1980) 2783–2792.
[23] J.K. Scott, S.L. Harris, L. Craig, J.-R. Marino-Albermas, F.-I. Auzanneau, K. Kenar, E.J. Toone, and B.M. Pinto, manuscript in preparation.